Available online at www.sciencedirect.com

SciVerse ScienceDirect

Ceramics International 38 (2012) 5915–5924

CERAMICS INTERNATIONAL

www.elsevier.com/locate/ceramint

Sol–gel synthesis and investigation of un-doped and Ce-doped strontium aluminates

M. Misevicius, O. Scit, I. Grigoraviciute-Puroniene, G. Degutis, I. Bogdanoviciene, A. Kareiva *

Department of General and Inorganic Chemistry, Vilnius University, Naugarduko 24, LT-03225 Vilnius, Lithuania

Received 29 February 2012; received in revised form 13 April 2012; accepted 13 April 2012
Available online 21 April 2012

Abstract

The preparation of various strontium aluminates including $SrAl_2O_4$ ($SrO–Al_2O_3$), $Sr_3Al_2O_6$ ($3SrO–Al_2O_3$), and $Sr_4Al_4O_{10}$ ($4SrO–2Al_2O_3$) was performed by using a simple aqueous sol–gel processing. The formation of strontium aluminate phases was investigated as a function of temperature in the range of 700–1200 °C. The obtained compounds were doped with cerium in the concentration range of 0.25–3.00 mol%. The sol–gel derived samples were characterized by X-ray powder diffraction (XRD) analysis, infrared spectroscopy (FTIR), scanning electron microscopy (SEM) and UV–Vis diffuse reflectance spectroscopy. It was demonstrated that optical properties of obtained phosphor materials slightly depend on the nature, crystal structure and phase purity of the strontium aluminate matrix.

Keywords: A. Sol–gel process; Strontium aluminates; Cerium doping; Chemical preparation

1. Introduction

The development of innovative multi-functional advanced materials should have a major impact in future applications. Different mixed-metal aluminate ceramics are promising materials for optical, electronic and structural applications [1–7]. For example, $LaAlO_3$ and related materials are currently being incorporated into automobile catalytic converters [8]. $LaAlO_3$ is promising substrate for the epitaxy of thin oxide films and has potential use as a buffer layer for the epitaxial growth of various perovskite-type films such as a high temperature superconductors, ferroelectrics and colossal magnetoresistance oxides [4,9,10]. Calcium aluminates are widely used in the steel and cement industry due to their relatively low density, hardness and straightness [11]. Magnesium aluminate spinels show interesting mechanical and refractory properties [12]. Aluminate materials could be successfully used as a solid oxide fuel cell functional anode material or highly conductive electrolyte [13,14].

The perovskite aluminates ($YAlO_3$, YAP) doped with lanthanide or transition elements offers advantages of longer lifetimes and higher, polarized cross sections with respect to most of other oxide matrices, and are useful as host for solid-state lasers, luminescence systems and window materials for a variety of lamps [15–17]. However, the discovery of advanced oxide phosphors with multiple superior qualities for display applications remains a difficult problem. The specific luminescence properties are highly sensitive to the changes in dopant composition and host nature as well [18,19]. Different aluminium garnet based materials are widely used in advanced optical technologies since garnets doped with a transition metal or lanthanide element exhibit outstanding luminescence properties [20–26]. The photoluminescence of lanthanide-doped alkaline earth aluminates having spinel crystal structure has attracted considerable attention in recent years owing to their very strong photoluminescence properties [27–29]. The luminescence properties of blue and green phosphors in more complicated aluminate matrixes were investigated for colour plasma display panel and fluorescent lights applications [30–33].

The lanthanide-doped strontium aluminates ($SrAl_2O_4$, $Sr_3Al_2O_6$, $SrAl_{12}O_{19}$, $SrAl_4O_7$ and $Sr_4Al_{14}O_{25}$) have attracted

* Corresponding author. Tel.: +370 5 2193110; fax: +370 5 2330987.
E-mail address: aivaras.kareiva@chf.vu.lt (A. Kareiva).

0272-8842/$36.00
http://dx.doi.org/10.1016/j.ceramint.2012.04.042

much attention since they show excellent properties such as high quantum efficiency, long persistence of phosphors and good stability when compared with other phosphorescent phosphors. These properties result in a wide application of these materials in many fields [34–53]. All mentioned properties of lanthanide-doped strontium aluminates are highly sensitive not only to the changes in dopant composition or host stoichiometry, but also to the processing conditions, which are very much responsible for the crystallinity, crystal shape, crystal size, crystal size distribution and phase purity of the resulting powders. In order to prepare these oxides, the solid state reaction method is still utilized [34,46,52,53]. However, this method, in general, requires extensive mechanical mixing and lengthy heat treatments in the temperature range of 1300–1600 °C. Moreover, different fluxing agents are used during the preparation of strontium aluminates using solid state reaction method. In order to overcome these inevitable disadvantages arising from the solid state reaction, some other methods have been also suggested. Several wet-chemical and/or soft chemistry techniques, such as the spray-drying preceramic processing [38], combustion synthesis [39,45,47,49], solvothermal reactions [48], or nonaqueous sol–gel process [42] have been used to produce strontium aluminate phases. Most of these methods suffer from the complex and time consuming procedures (long refluxing times, gelation periods of several days, etc.) and/or mismatch in the solution behaviour of the constituents. As a consequence, gross inhomogeneities may be present in the obtained ceramics e.g., significant amounts of impurity phases may form. Owing to such a wide and diverse application potential of strontium aluminate-based ceramics, new routes for the synthesis of various strontium aluminates are highly desirable.

Over the last few decades, the sol–gel techniques have been used to prepare a variety of mixed-metal oxides, nanomaterials and nanoscale architectures, nanoporous oxides, and organic–inorganic hybrids [54–57]. Aqueous sol–gel methods based on molecular precursors have a cutting edge over the other solution routes because they allow chemical interactions among the precursor species of the initial mixture favouring the evolution of a homogeneous solid-state structure at the atomic level [58]. However, only one sol–gel synthesis route is suggested for the preparation of europium and praseodymium doped $Sr_3Al_2O_6$ phosphors [43,44], to the best our knowledge. In this study we present results of a systematic study of aqueous sol–gel synthetic approach to pure and Ce-doped strontium aluminates $SrAl_2O_4$, $Sr_3Al_2O_6$, $Sr_4Al_4O_{10}$, $SrAl_{12}O_{19}$ and $Sr_4Al_{14}O_{25}$ using glycolate intermediates.

2. Experimental procedure

Strontium aluminate $SrAl_2O_4$, $Sr_3Al_2O_6$, $Sr_4Al_4O_{10}$, $SrAl_{12}O_{19}$ and $Sr_4Al_{14}O_{25}$ ceramic samples were synthesized by aqueous sol–gel method. The gels were prepared using stoichiometric amounts of analytical-grade $Sr(CH_3COO)_2$ and $Al(NO_3)_3{\cdot}9H_2O$ as starting materials. For the preparation of un-doped samples by the sol–gel process, strontium acetate was first dissolved in CH_3COOH (50 ml, 0.2 M) at 60 °C. To this solution, aluminium nitrate dissolved in 50 ml of distilled water was added and the resulting mixture was stirred for 1 h at the same temperature. For the preparation of Ce-doped samples (Ce = 0.25, 0.50, 0.75, 1.00, 2.00 and 3.00 mol%) the appropriate amount of $Ce(NO_3)_3{\cdot}6H_2O$ dissolved in 50 ml of 0.2 M CH_3COOH at 60 °C was added and the resulting mixture was stirred for 1 h at the same temperature. In a following step, 1,2-ethanediol ($HOCH_2CH_2OH$) (2 ml) as complexing agent was added to the reaction solution. After concentrating the solutions by a slow evaporation at 65 °C under stirring, the Sr(Ce)–Al–O acetate–nitrate–glycolate sols turned into white translucent gels. The oven dried (100 °C) gel powders were ground in an agate mortar and preheated for 5 h at 700 °C in air. Since the gels are very combustible, a slow heating rate (∼3–4 °C min^{-1}) especially between 100 and 400 °C was found to be essential. After an intermediate grinding in an agate mortar, the powders were additionally sintered in air for 10 h at 700–1200 °C.

Powder X-ray diffraction (XRD) measurements were performed at room temperature on a DS Bruker AXS diffractometer (Cu K(radiation: λ = 1.5418 Å). The infrared spectra in the range of 4000–400 cm^{-1} were recorded on Perkin-Elmer FT-IR Spectrum BX II FTIR spectrometer. Samples were prepared as KBr pellets (1.5%). Scanning electron microscopy (SEM) was used to study the morphology of the samples. The SEM analysis was performed under vacuum in the specimen chamber of scanning electron microscope EVO 50 XVP. The UV–Vis diffuse reflectance spectra were recorded on Perkin-Elmer Lambda 35 UV-Vis spectrophotometer with an integrated 50 mm sphere attachment.

3. Results and discussion

3.1. Sol–gel derived un-doped strontium aluminates

The XRD patterns of the Sr–Al–O acetate–nitrate–glycolate gels which correspond to the nominal chemical composition of $SrAl_2O_4$ and heated from 700 to 1200 °C for 10 h are shown in Fig. 1. The diffraction patterns of the obtained powders at 700 °C were broad due to the amorphous character of the synthesized systems. However, the formation of few crystalline phases ($Sr_3Al_2O_6$, $SrCO_3$ and unknown) could be detected from the XRD pattern. The phase composition of the samples obtained at 800–1200 °C were qualitatively the same regardless the annealing temperature. Additionally the formation of spinel crystal structure strontium aluminate starts at 800 °C. The XRD pattern of the sample heated at 1100 °C shows the formation $SrAl_2O_4$ and $Sr_3Al_2O_6$ crystalline phases. According to XRD analysis, synthesis performed at 1200 °C yields monophasic crystalline monoclinic $SrAl_2O_4$ sample (PDF [34-379]].

The XRD patterns of Sr–Al–O precursor powders which correspond to the nominal chemical composition of $Sr_3Al_2O_6$ and sintered from 700 to 1200 °C for 10 h are shown in Fig. 2. According to the XRD analysis, the formation of $Sr_3Al_2O_6$ along with $SrCO_3$ has started already at 700 °C. Fully crystallized single-phase oxide $Sr_3Al_2O_6$ with well pronounced

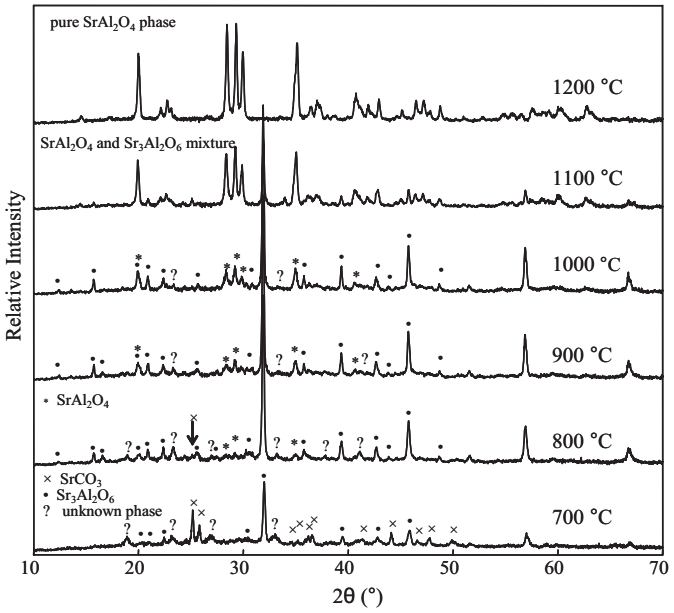

Fig. 1. XRD patterns of sol–gel derived $SrAl_2O_4$ synthesized at different temperatures.

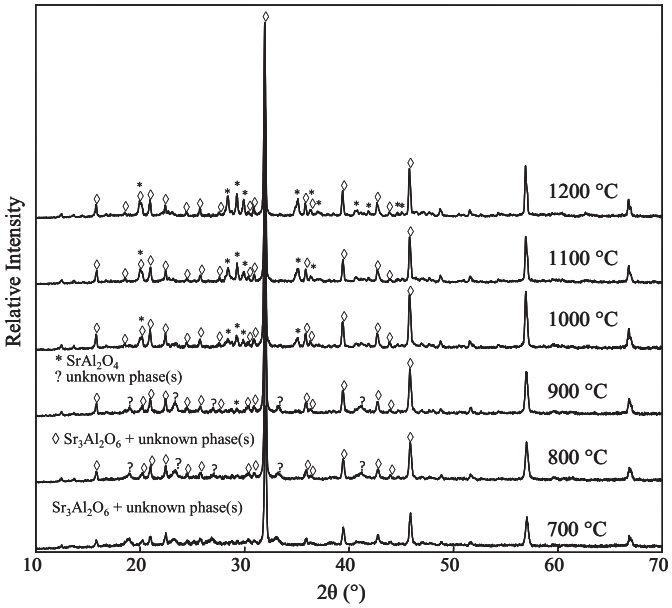

Fig. 3. XRD patterns of sol–gel derived $Sr_4Al_4O_{10}$ synthesized at different temperatures.

cubic crystal structure has formed already at 800 °C (PDF [24-1187]). The XRD patterns of this sample calcined in the temperature range of 800–1200 °C confirmed $Sr_3Al_2O_6$ to be the only one crystalline component.

The attempts to prepare the $Sr_4Al_4O_{10}$ phase using the same sol–gel technique were also performed. Fig. 3 presents the XRD patterns of Sr–Al–O gel precursors which correspond to the nominal chemical composition of $Sr_4Al_4O_{10}$ and sintered from 700 to 1200 °C for 10 h. However the formation of $Sr_4Al_4O_{10}$ phase does not proceed in whole temperature range. The X-ray diffraction patterns of the samples obtained at 700–800 °C show lines which could be attributed to the $Sr_3Al_2O_6$ and unknown phases. With further increasing temperature up to 900 °C the diffraction line attributable to the $SrAl_2O_4$ phase appears in the X-ray diffraction pattern of the ceramic sample. The diffraction lines assignable only to the $SrAl_2O_4$ and $Sr_3Al_2O_6$ phases are well pronounced in the diffraction patterns recorded for the samples annealed at higher temperatures (1000–1200 °C). Thus, the formation of the biphasic mixture such as $SrAl_2O_4/Sr_3Al_2O_6$ instead of $Sr_4Al_4O_{10}$ is evident from XRD analysis data.

The impurity phases ($SrCO_3$, $SrAl_2O_4$, Al_2O_3 and unknown) were the dominating components during the synthesis of $SrAl_{12}O_{19}$ ceramics in the temperature range of 700–1000 °C

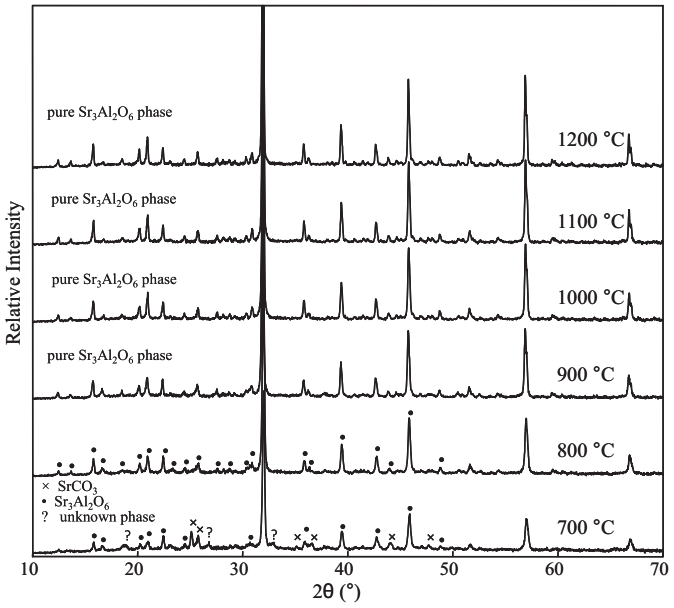

Fig. 2. XRD patterns of sol–gel derived $Sr_3Al_2O_6$ synthesized at different temperatures.

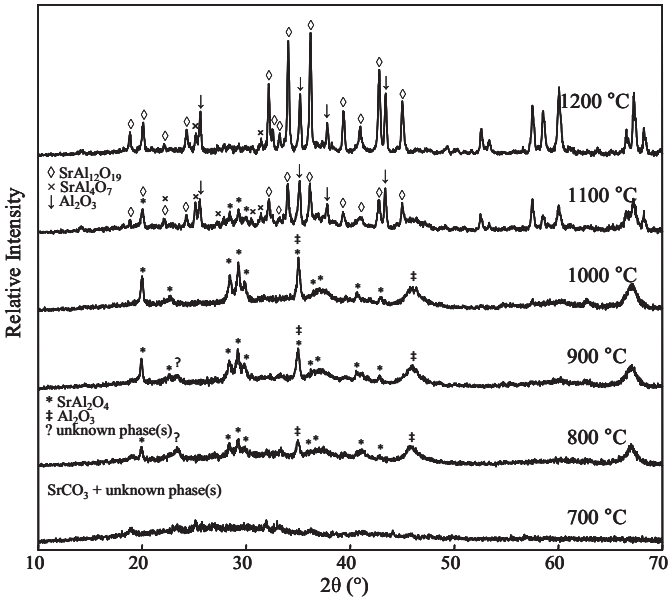

Fig. 4. XRD patterns of sol–gel derived $SrAl_{12}O_{19}$ synthesized at different temperatures.

(Fig. 4). The X-ray diffraction peaks are consistent with the main diffractions of hexagonal $SrAl_{12}O_{19}$ (PDF [26-976]), monoclinic $SrAl_4O_7$ (PDF [25-1208]) and rhombohedral corundum Al_2O_3 (PDF [46-1212]) phases when the crystallization process was performed at 1100 °C. Apparently, the amount of $SrAl_{12}O_{19}$ phase increases with increasing sintering temperature up to 1200 °C, however alumina and minor amount of $SrAl_4O_7$ still exist in the synthesis product. Possibly $SrAl_2O_4$ reacts with Al_2O_3 at 1000 °C according to the reaction:

$$SrAl_2O_4 + Al_2O_3 \rightarrow SrAl_4O_7 \quad (1)$$

The formed $SrAl_4O_7$ reacts with remaining $SrAl_2O_4$ and Al_2O_3 at 1100 °C by two possible solid state reactions [59]:

$$SrAl_2O_4 + SrAl_4O_7 + 9Al_2O_3 \rightarrow 2SrAl_{12}O_{19} \quad (2)$$

$$2SrAl_2O_4 + SrAl_4O_7 + 14Al_2O_3 \rightarrow 3SrAl_{12}O_{19} \quad (3)$$

Fig. 5 shows the XRD patterns of Sr–Al–O gel precursors which correspond to the nominal chemical composition of $Sr_4Al_{14}O_{25}$ and sintered from 700 to 1200 °C for 10 h. The broad peaks in the resulting powder patterns and poor intensities suggest that a considerable amount of the material ($SrCO_3$ + $SrAl_2O_4$) obtained at low temperatures (700–800 °C) is either amorphous or nanocrystalline [60]. At 900 °C, the XRD powder patterns show no evidence for the formation of crystalline carbonate species. At this stage the synthesis product contains three crystalline phases $SrAl_2O_4$, $SrAl_4O_7$ and $Sr_3Al_2O_6$. With further increasing the temperature, however, the formation of perovskite aluminate $Sr_4Al_{14}O_{25}$ using this sol–gel chemistry approach seems to be problematic.

FTIR analysis of synthesized samples is important both for the control of the reaction process and the properties of materials obtained. Fig. 6 shows the FTIR spectra of $SrAl_2O_4$ ceramics obtained at 800 and 1200 °C. The synthesized ceramics show several intense broad bands. Strong absorption

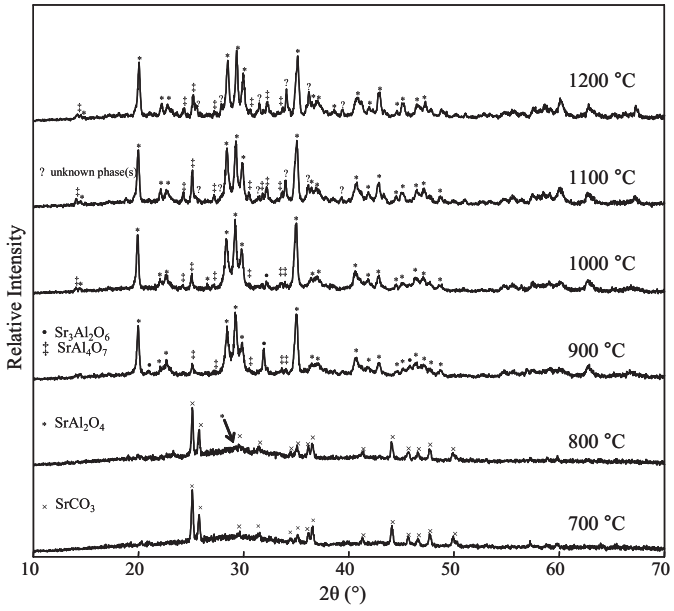

Fig. 5. XRD patterns of sol–gel derived $Sr_4Al_{14}O_{25}$ synthesized at different temperatures.

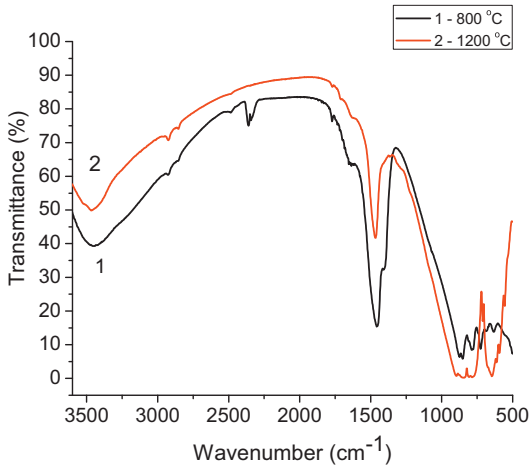

Fig. 6. FTIR spectra of $SrAl_2O_4$ synthesized at different temperatures.

bands arising from O–H stretching and bending vibration of water due to the exposure of the samples to the atmosphere occur at ~3500–3400 and ~1600 cm^{-1}, respectively [61]. Importantly, in the 1000–500 cm^{-1} fingerprint region, several sharp bands are typical metal–oxygen absorptions (Sr–O and Al–O stretching frequencies), probably characteristic for the spinel-type compounds [62]. In Fig. 6, the spectra of strontium aluminate samples show the strong peaks at ~1500 cm^{-1}. The exact origin of this peak, however, is not very clear. It is known, that typical carbonate vibrations are ~1470–1390 cm^{-1} (triply degenerated stretching mode) and ~880–850 cm^{-1} (doubly degenerated stretching mode) [63]. So, the bands located at ~1500 cm^{-1} could not be assigned to the metal carbonates formed as intermediates during high-temperature treatments. It is well known that aluminium and strontium carbonates ($Al_2(CO_3)_3$ and $SrCO_3$) decomposes at lower temperatures [60,64,65].

The FTIR spectra of $Sr_3Al_2O_6$ samples synthesized at different temperatures are shown in Fig. 7. The envelope of three broad absorption bands in the region of 1000–500 cm^{-1} presented in Fig. 7 is well resolved. The both FTIR spectra of

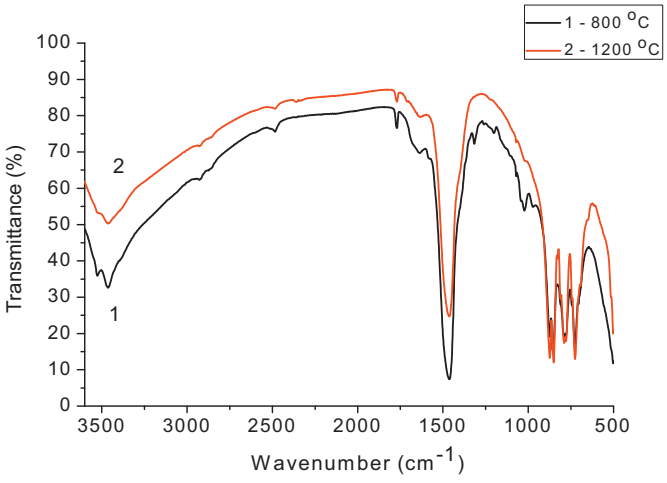

Fig. 7. FTIR spectra of $Sr_3Al_2O_6$ synthesized at different temperatures.

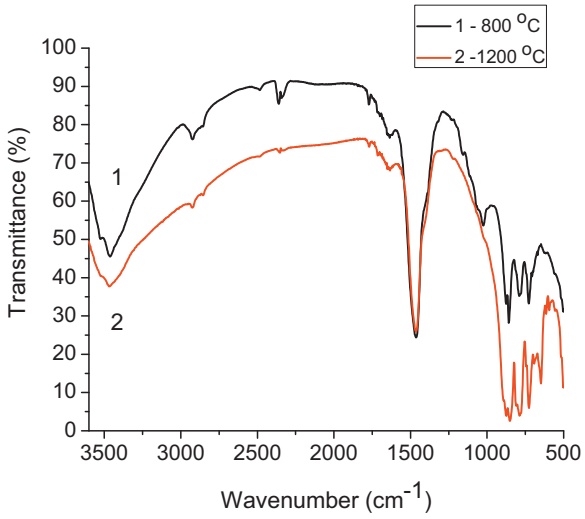

Fig. 8. FTIR spectra of $Sr_4Al_4O_{10}$ synthesized at different temperatures.

$Sr_3Al_2O_6$ samples are almost identical. Besides, they are very similar to FTIR spectra of $SrAl_2O_4$ ceramics. The spectra of $Sr_3Al_2O_6$ samples also show the strong peaks at ~1500 cm^{-1}. However, the existence of non-decomposed metal carbonates in the product synthesized at 1200 °C temperature is not possible. It is not surprising, that FTIR spectra of $Sr_4Al_4O_{10}$ samples synthesized at different temperatures (see Fig. 8) are very similar to previous ones. The fact is that during the sol–gel synthesis of $Sr_4Al_4O_{10}$ the mixture of two phases ($SrAl_2O_4$ and $Sr_3Al_2O_6$) has formed. Therefore, the FTIR results partially support the conclusions made on grounds of the XRD measurements. However, the question about the nature of the bands located at ~1500 cm^{-1} in the FTIR spectra of sol–gel derived strontium aluminates should be answered in future.

Moreover, these observations are thoroughly supported by the scanning electron microscopy studies. The SEM images of $SrAl_2O_4$ ceramics calcined at 800 and 1200 °C are shown in Fig. 9. The cloudy particles obtained at 800 °C seem to be micro-sized amorphous solids with particle size about ~10–15 μm and they are partially fused to form hard agglomerates (~30–50 μm in size). With increasing temperature up to 1200 °C the formation plate-like crystals with regular size is evident, i.e. the SEM images revealed agglomerated grains of different size ranging from 1 μm to 2 μm. The particle size does not change and no progressive change in morphology was observed with changing chemical composition or crystal structure of sol–gel derived strontium aluminates. Figs. 10 and 11 show the surface features of the $Sr_3Al_2O_6$ and $Sr_4Al_4O_{10}$ powders calcined at different temperatures, respectively. From these SEM images it is evident that $Sr_3Al_2O_6$ and $Sr_4Al_4O_{10}$ powders are also composed of plate-like crystallites having a similar size and the tendency to form agglomerates. The samples annealed at higher temperature exhibit clustered grains

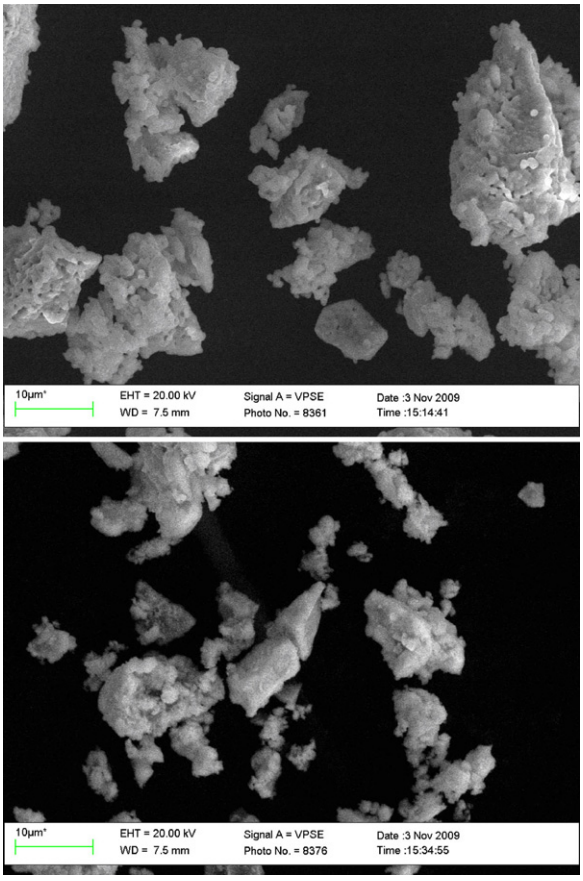

Fig. 9. SEM micrographs of $SrAl_2O_4$ ceramics annealed at 800 °C (at bottom) and 1200 °C (at top). Magnification: 5000×.

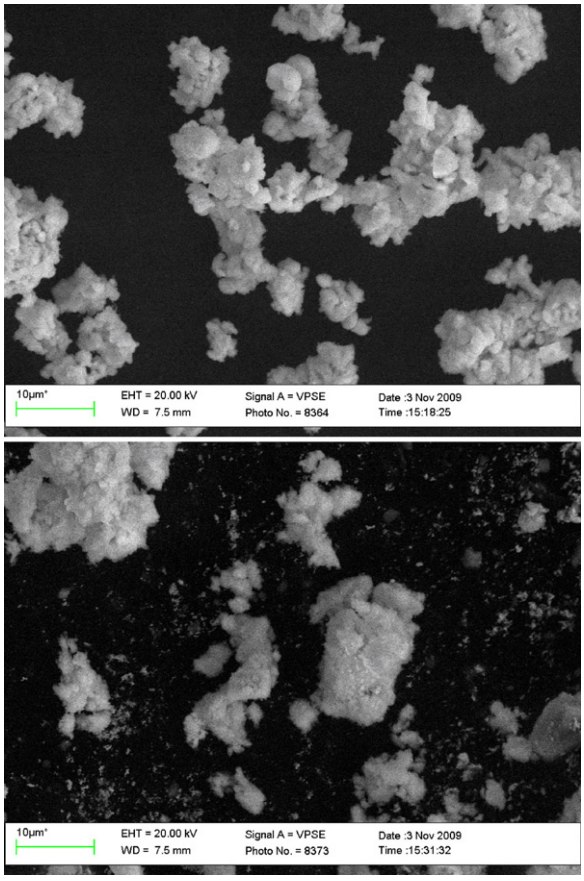

Fig. 10. SEM micrographs of $Sr_3Al_2O_6$ ceramics annealed at 800 °C (at bottom) and 1200 °C (at top). Magnification: 5000×.

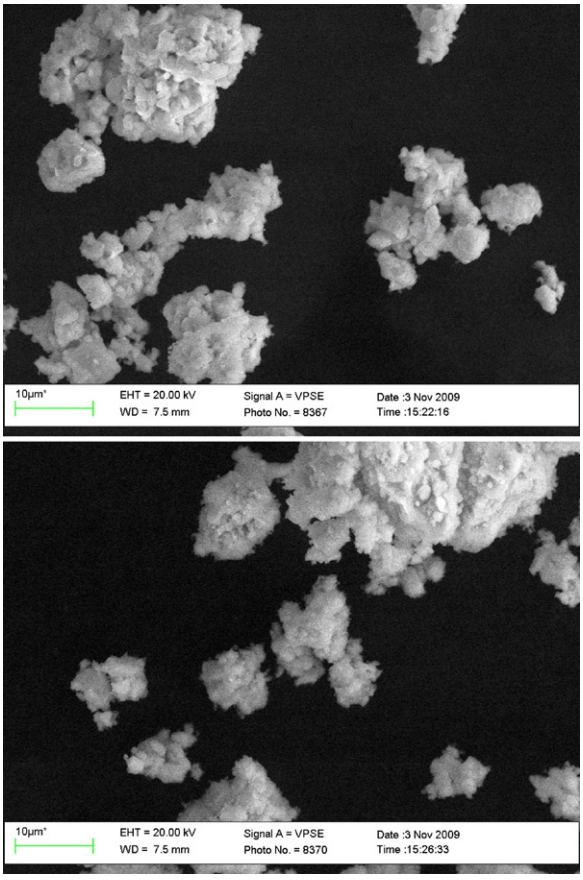

Fig. 11. SEM micrographs of $Sr_4Al_4O_{10}$ ceramics annealed at 800 °C (at bottom) and 1200 °C (at top). Magnification: 5000×.

made up of several tiny crystallites with a defined microstructure (Figs. 10 and 11).

3.2. Sol–gel derived Ce-doped strontium aluminates

As was mentioned above, during the sol–gel processing of $SrAl_{12}O_{19}$ and $Sr_4A_{l4}O_{25}$ the multiphasic crystalline mixtures were obtained by heating Sr–Al–O precursor gels in the temperature range of 700–1200 °C. Therefore, for the preparation of cerium-doped strontium aluminate samples only three matrixes $SrAl_2O_4$, $Sr_3Al_2O_6$ and $Sr_4Al_4O_{10}$ ($Sr_3Al_2O_6 + SrAl_2O_4$) were selected. The Ce-doped samples $SrAl_2O_4$:Ce_x, $Sr_3Al_2O_6$:Ce_x and "$Sr_4Al_4O_{10}$:Ce_x" were synthesized with different concentrations of cerium (Ce = 0.25, 0.50, 0.75, 1.00, 2.00 and 3.00 mol%). The XRD patterns of the $SrAl_2O_4$:Ce_x specimens annealed at 1200 °C temperature for 10 h are shown in Fig. 12. As seen, in all cases the $SrAl_2O_4$:Ce_x phase is dominating and only minor amount of impurity phases has formed. The XRD patterns of $SrAl_2O_4$:Ce_x samples with smaller concentrations of cerium (0.25–1.00 mol%) contained additional peak located at approximately $2\theta \approx 32°$. However we were not able to attribute this peak to any crystalline phase. Interestingly, this peak disappeared with further increasing concentration of cerium in $SrAl_2O_4$:Ce_x. On the other hand, the XRD patterns of $SrAl_2O_4$:Ce_x samples with higher concentrations of cerium (2.00–3.00 mol%) showed the negligible

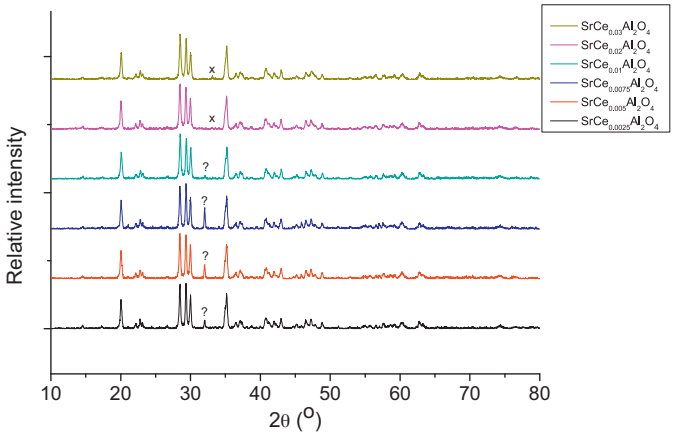

Fig. 12. XRD patterns of $SrAl_2O_4$:Ce_x ceramic samples synthesized at 1200 °C. The concentration of cerium from bottom to the top is Ce = 0.25, 0.50, 0.75, 1.00, 2.00 and 3.00 mol%. Impurity phases: (?) unknown; (×) CeO_2.

formation of CeO_2 phase (PDF [034-0394]). The small diffraction peaks attributable to ceria phase are visible at $2\theta \approx 33°$.

The XRD patterns of $Sr_3Al_2O_6$:Ce_x powders sintered at 850 °C for 10 h are shown in Fig. 13. Fully crystallized single-phase cerium-doped strontium aluminate $Sr_3Al_2O_6$ has formed in whole doping range. Fig. 14 presents the XRD patterns of $Sr_4Al_4O_{10}$:Ce_x samples annealed at 1000 °C for 10 h. Again, the formation of mixture of two crystalline phases $SrAl_2O_4$ and $Sr_3Al_2O_6$ instead of $Sr_4Al_4O_{10}$ in whole concentration range of dopant element is evident. Surprisingly, no any impurity phases could be detected as was determined during the synthesis of $SrAl_2O_4$:Ce_x samples. These results let us to conclude that successful cerium doping was achieved in the concentration range of 0.25–1.00 mol% Ce during the sol–gel synthesis of $SrAl_2O_4$ and in the concentration range of 0.25–3.00 mol% when $Sr_3Al_2O_6$ or $Sr_4Al_4O_{10}$ ($Sr_3Al_2O_6 + SrAl_2O_4$) were synthesized.

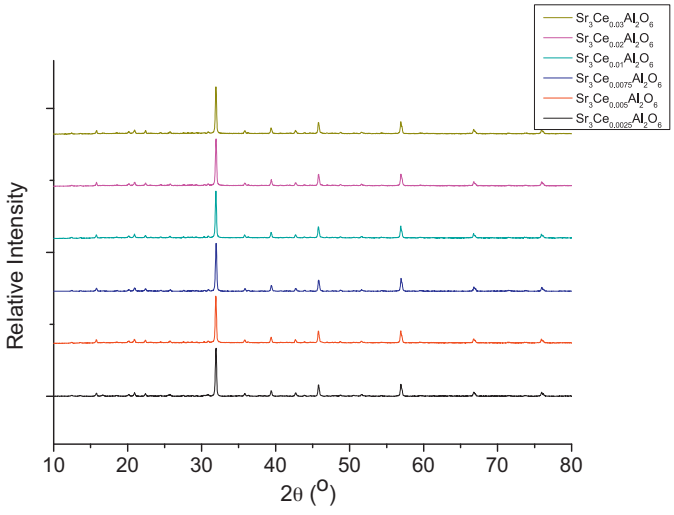

Fig. 13. XRD patterns of $Sr_3Al_2O_6$:Ce_x ceramic samples synthesized at 850 °C. The concentration of cerium from bottom to the top is Ce = 0.25, 0.50, 0.75, 1.00, 2.00 and 3.00 mol%.

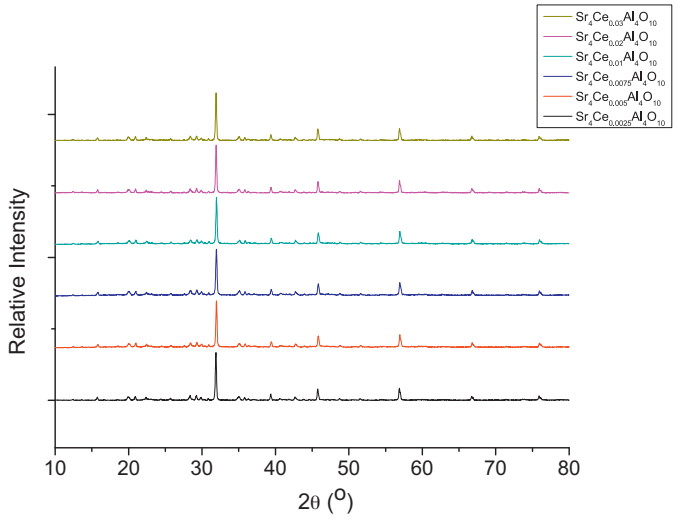

Fig. 14. XRD patterns of "$Sr_4Al_4O_{10}$:Ce_x" ceramic samples synthesized at 1000 °C. The concentration of cerium from bottom to the top is Ce = 0.25, 0.50, 0.75, 1.00, 2.00 and 3.00 mol%. The formation of mixture of two crystalline phases $Sr_3Al_2O_6$ and $SrAl_2O_4$ is evident.

The particle size and the main morphological features did not change with doping of sol–gel derived strontium aluminates with different concentrations of cerium. The SEM images showed that $SrAl_2O_4$:Ce_x, $Sr_3Al_2O_6$:Ce_x and "$Sr_4Al_4O_{10}$:Ce_x" powders are also composed of plate-like crystallites having a similar size and the tendency to form aggregates.

The optical reflectance spectra of $SrAl_2O_4$:Ce_x, $Sr_3Al_2O_6$:Ce_x and "$Sr_4Al_4O_{10}$:Ce_x" powders were measured at room temperature in the range of 250–800 nm. All the samples exhibit a high transmittance in the visible region. Fig. 15 demonstrates the reflectance spectra of $SrAl_2O_4$:Ce_x ceramic powders produced by sol–gel method. As seen from Fig. 15, the reflection spectra qualitatively are almost identical regardless the substitutional level of cerium. In UV range the strontium aluminate samples show a significant increase of reflection up to 400 nm. From this point the reflection is almost constant, i.e. not wavelength dependent, and close to unity, which proves the high optical quality of the $SrAl_2O_4$:Ce_x samples. However, broad absorption bands could be detected between 575 nm and 700 nm. These results clearly show that optical properties of $SrAl_2O_4$:Ce_x are quite different from the Ce-doped garnet samples [24,66,67]. In the case of garnet materials, from 400 nm the reflection abruptly decreases and again increases starting from 455 nm. And only in the higher wavelength region (from ~545 nm) the reflection is almost constant.

Fig. 16 shows optical reflectance spectra of $Sr_3Al_2O_6$:Ce_x ceramic powders. As seen from Fig. 16, the absorption edge for the $Sr_3Al_2O_6$:Ce_x samples could be detected at around 300 nm as was observed in the case of $SrAl_2O_4$:Ce_x specimens. As seen, the $Sr_3Al_2O_6$:Ce_x samples also show a significant increase of reflection up to 400 nm. However, from this point the reflection is not constant but increases monotonically till 585 nm. Broad absorption bands could be detected between 585 nm and 675 nm. Thus, the observed absorption region for the $Sr_3Al_2O_6$:Ce_x samples is narrower in comparison with cerium-doped spinel aluminates. Moreover, for the sample with highest concentration of cerium ($Sr_3Al_2O_6$:$Ce_{0.03}$) the absorption band in the range of 585–675 nm is missing. The obtained results clearly show the influence of strontium aluminate matrix on the optical properties of the synthesized phosphors from Fig. 17.

As seen, the optical reflectance spectra of "$Sr_4Al_4O_{10}$:Ce_x" synthesized by sol–gel route are slightly shifted towards those presented in Figs. 15 and 16. These results are quite consequent since according to XRD data the "$Sr_4Al_4O_{10}$:Ce_x" matrix actually is a mixture of $SrAl_2O_4$:Ce_x and $Sr_3Al_2O_6$:Ce_x phases. On the other hand, the reflectance spectra of "$Sr_4Al_4O_{10}$:Ce_x" are not linear sum of two reflectance spectra of $SrAl_2O_4$:Ce_x and $Sr_3Al_2O_6$:Ce_x. The clearly expressed more intensive broad absorption bands which cover from 550 to 700 nm and peaking

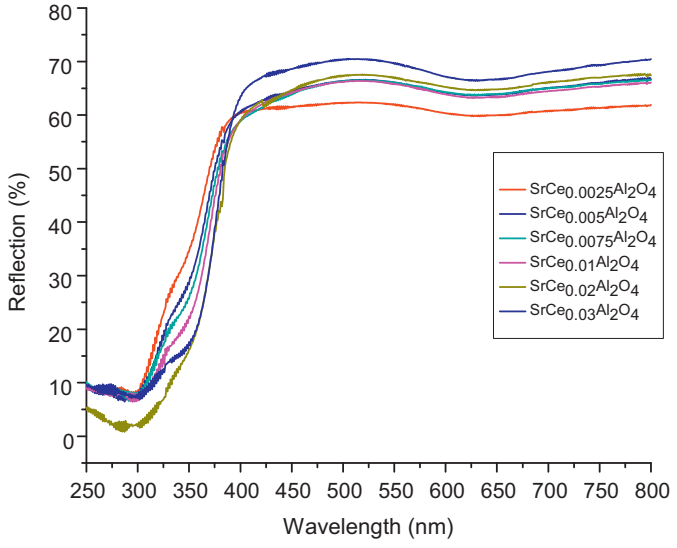

Fig. 15. Reflection spectra of $SrAl_2O_4$:Ce_x samples as a function of Ce concentration.

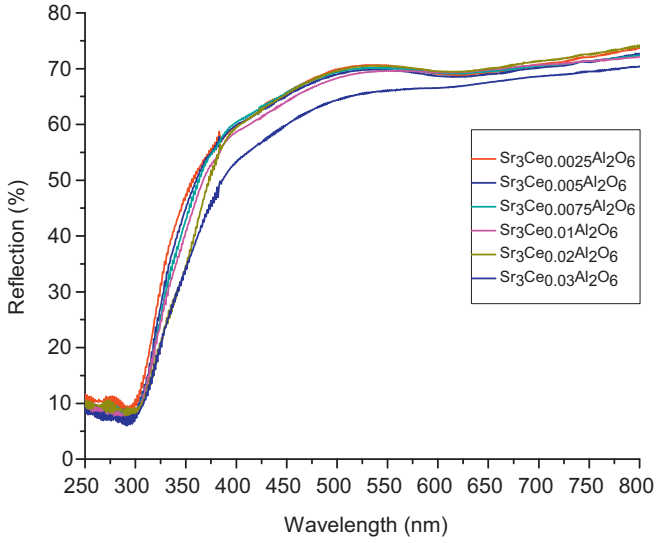

Fig. 16. Reflection spectra of $Sr_3Al_2O_6$:Ce_x samples as a function of Ce concentration.

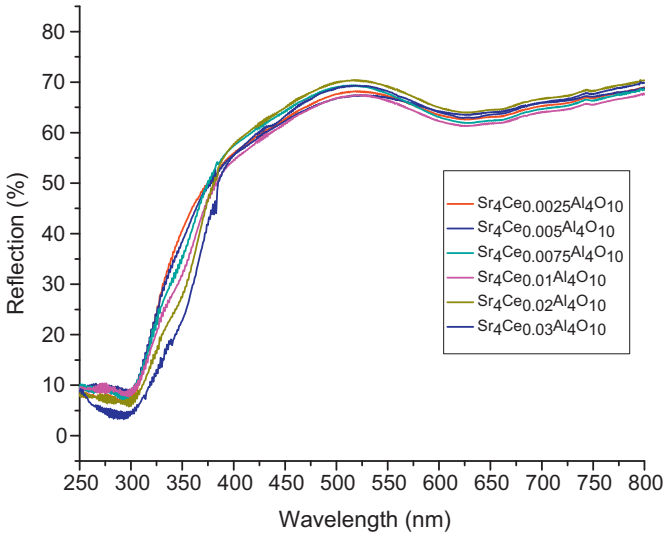

Fig. 17. Reflection spectra of "$Sr_4Al_4O_{10}$:Ce_x" samples as a function of Ce concentration.

at ~615 nm observed for the "$Sr_4Al_4O_{10}$:Ce_x" samples prove our last conclusion. Besides, the reflection spectra of "$Sr_4Al_4O_{10}$:Ce_x" samples qualitatively are also almost identical regardless the substitutional level of cerium. The absorption of synthesized phosphors is shifted towards longer wavelengths to compare with YAG:Ce. The present fact possibly indicates that the lowest 5d orbital of Ce^{3+} in strontium aluminate host lattices lies at low energies than in YAG:Ce. Usually the Ce^{3+} emission is in the ultraviolet or blue spectral region, but in $Y_3Al_5O_{12}$ it is in the green and red (crystal-field effect), and in CaS in the red (covalency effect) [68]. The observed shift of emission in strontium aluminates also could be associated with occurrence of different defects [69]. Finally, high phase purity and broad transparent range of $SrAl_2O_4$:Ce_x, $Sr_3Al_2O_6$:Ce_x and "$Sr_4Al_4O_{10}$:Ce_x" samples synthesized by sol–gel method make these compounds excellent candidates as host material for advanced optical applications.

4. Conclusion

For the preparation of strontium aluminate $SrAl_2O_4$, $Sr_3Al_2O_6$, $Sr_4Al_4O_{10}$, $SrAl_{12}O_{19}$ and $Sr_4Al_{14}O_{25}$ ceramic samples an aqueous sol–gel method has been suggested. According to XRD analysis, synthesis performed at 1200 °C yielded monophasic crystalline monoclinic $SrAl_2O_4$ sample. Fully crystallized single-phase oxide $Sr_3Al_2O_6$ with well pronounced cubic crystal structure, however, has formed already at 800 °C. Interestingly, the formation of the biphasic mixture such as $SrAl_2O_4$/$Sr_3Al_2O_6$ instead of $Sr_4Al_4O_{10}$ was evident from XRD analysis data. It was demonstrated, that the amount of $SrAl_{12}O_{19}$ phase increased with increasing sintering temperature up to 1200 °C, however alumina and minor amount of $SrAl_4O_7$ have formed as impurity phases as well. The formation of perovskite aluminate $Sr_4Al_{14}O_{25}$ in the temperature range of 700–1200 °C using this sol–gel chemistry approach seems to be problematic. The FTIR and SEM results partially supported the conclusions made on grounds of the XRD measurements. Also, the Ce-doped samples $SrAl_2O_4$:Ce_x, $Sr_3Al_2O_6$:Ce_x and $Sr_4Al_4O_{10}$:Ce_x with different concentrations of cerium were successfully synthesized by this sol–gel method. The particle size and the main morphological features did not change with doping of sol–gel derived strontium aluminates with different concentrations of cerium. The optical reflectance spectra of $SrAl_2O_4$:Ce_x, $Sr_3Al_2O_6$:Ce_x and "$Sr_4Al_4O_{10}$:Ce_x" powders measured at room temperature in the range of 250–800 nm clearly showed the influence of strontium aluminate matrix on the optical properties of the synthesized phosphors. In the view of the above results and the increasing importance of the optical materials, the Ce-doped strontium aluminate samples show a considerable application potential.

Acknowledgement

O. Scit is grateful for the National Grant from Research Council of Lithuania for Postdoctoral studies (SF-PD-2010-08-10-0228).

References

[1] M. Yada, M. Ohya, M. Machida, T. Kijima, Synthesis of porous yttrium aluminium oxide templated by dodecyl sulfate assemblies, Chemical Communications (1998) 1941–1942.
[2] M.A. Gulgun, V. Putlayev, M. Ruhle, Effects of yttrium doping α-alumina. I. Microstructure and microchemistry, Journal of the American Ceramic Society 82 (1999) 1849–1856.
[3] B. Jancar, D. Suvorov, M. Valant, G. Drazic, Characterization of $CaTiO_3$–$NdAlO_3$ dielectric ceramics, Journal of the European Ceramic Society 23 (2003) 1391–1400.
[4] P.D. Tall, C. Coupeau, J. Rabier, Indentation-induced twinning in $LaAlO_3$ single crystals: an atomic force microscopy study, Scripta Materialia 49 (2003) 903–908.
[5] S. Zha, J. Cheng, Y. Liu, X. Liu, G. Meng, Electrical properties of pure and Sr-doped $Bi_2Al_4O_9$ ceramics, Solid State Ionics 156 (2003) 197–200.
[6] J. Zylberberg, Z.-G. Ye, Improved dielectric properties of bismuth-doped $LaAlO_3$, Journal of Applied Physics 100 (2006) 086102.
[7] W. Lei, W.-Z. Lu, X.-C. Wang, Temperature compensating $ZnAl_2O_4$–Co_2TiO_4 spinel-based low-permittivity microwave dielectric ceramics, Ceramics International 38 (2012) 99–103.
[8] D.A. Atwood, B.C. Yearwood, The future of aluminum chemistry, Journal of Organometallic Chemistry 600 (2000) 186–197.
[9] M. Nieminen, T. Sajavaara, E. Rauhala, M. Putkonen, L. Niinistö, Surface-controlled growth of $LaAlO_3$ thin films by atomic layer epitaxy, Journal of Materials Chemistry 11 (2001) 2340–2345.
[10] D.I. Savytskii, A.O. Matkovskii, I.M. Solskii, F. Wallrafen, A. Suchocki, L.O. Vasylechko, S.B. Ubizskii, Etching figures in neodymium gallate and yttrium aluminate crystals, Crystal Research and Technology 35 (2000) 197–205.
[11] M.A. Rodriguez, C.L. Aguilar, M.A. Aghayan, Solution combustion synthesis and sintering behaviour of $CaAl_2O_4$, Ceramics International 38 (2012) 395–399.
[12] N.M. Khalil, M.B. Hassan, E.M.M. Ewais, F.A. Saleh, Sintering, mechanical and refractory properties of MA spinel prepared via co-precipitation and sol–gel techniques, Journal of Alloys and Compounds 496 (2010) 600–607.
[13] S.A. Venancio, P.E.V. de Miranda, Synthesis of $CeAlO_3$/CeO_2–Al_2O_3 for use as a solid oxide fuel cell functional anode material, Ceramics International 37 (2011) 3139–3152.
[14] K.Z. Fung, T.Y. Chen, Cathode-supported SOFC using a highly conductive lanthanum aluminate-based electrolyte, Solid State Ionics 188 (2011) 64–68.

[15] M. Malinowski, R. Piramidowicz, Z. Frukacz, G. Chadeyron, R. Mahiou, M.F. Joubert, Spectroscopy and upconversion processes in $YAlO_3$:Ho^{3+} crystals, Optical Materials 12 (1999) 409–423.

[16] Y. Zhydachevskii, A. Durygin, A. Suchocki, A. Matkovskii, D. Sugak, G.B. Loutts, M.A. Noginov, Radiation and thermally induced effects in $YAlO_3$:Mn crystals, Journal of Luminescence 109 (2004) 39–49.

[17] L. Luo, Q.F. Liu, Q. Liu, Synthesis and luminescent properties of $GdAlO_3$:RE by combustion process, Journal of Rare Earths 22 (2004) 268–271.

[18] T.X. Sun, Combinatorial search for advanced luminescence materials, Biotechnology and Bioengineering (Combinatorial Chemistry) 61 (1999) 193–201.

[19] I. Muliuoliene, S. Mathur, D. Jasaitis, H. Shen, V. Sivakov, R. Rapalaviciute, A. Beganskiene, A. Kareiva, Evidence of the formation of mixed-metal garnets via sol–gel synthesis, Optical Materials 22 (2003) 241–250.

[20] D. Pawlak, Z. Frukacz, Z. Mierczyk, A. Suchocki, J. Zachara, Spectroscopic and crystallographic studies of YAG:Pr^{4+} single crystals, Journal of Alloys and Compounds 275–277 (1998) 361–364.

[21] A. Lupei, V. Lupei, V.N. Enaki, C. Presura, A. Petraru, Electron–phonon coupling for heavy RE^{3+} ions in crystals, Spectrochimica Acta Part A 55 (1999) 773–781.

[22] D. Hreniak, W. Strek, Synthesis and optical properties of Nd^{3+}-doped $Y_3Al_5O_{12}$ nanoceramics, Journal of Alloys and Compounds 341 (2002) 183–186.

[23] X.Y. Pan, M.M. Wu, Q. Su, Comparative investigation on synthesis and photoluminescence of YAG:Ce phosphor, Materials Science and Engineering B 106 (2004) 251–256.

[24] A. Katelnikovas, T. Justel, D. Uhlich, J.-E. Jorgensen, S. Sakirzanovas, A. Kareiva, Characterization of cerium-doped yttrium aluminium garnet nanopowders synthesized via sol–gel process, Chemical Engineering Communications 195 (2008) 758–769.

[25] Y. Matsui, H. Horikawa, M. Iwasaki, W. Park, Preparation of YAG:Ce nanocrystals by an environmentally friendly wet process. Effect of Ce(3+) concentration on photoluminescent property, Journal of Ceramic Processing Research 12 (2011) 348–351.

[26] P. Rai, M.-K. Song, H.-M. Song, J.-H. Kim, Y.-S. Kim, I.-H. Lee, Y.-T. Yu, Synthesis, growth mechanism and photoluminescence of monodispersed cubic shape Ce doped YAG nanophosphor, Ceramics International 38 (2012) 235–242.

[27] T. Aitasalo, J. Holsa, H. Jungner, M. Lastusaari, J. Niittykoski, Mechanisms of persistent luminescence in Eu^{2+}, RE^{3+} doped alkaline earth aluminates, Journal of Luminescence 94 (2001) 59–63.

[28] T. Aitasalo, J. Holsa, H. Jungner, M. Lastusaari, J. Niittykoski, Sol–gel processed Eu^{2+}-doped alkaline earth aluminates, Journal of Alloys and Compounds 341 (2002) 76–78.

[29] H.-S. Roh, I.-S. Cho, J.-S. An, C.M. Cho, T.H. Noh, D.K. Yim, D.-W. Kim, K.S. Hong, Enhanced photoluminescence property of Dy^{3+} co-doped $BaAl_2O_4$:Eu^{2+} green phosphor, Ceramics International 38 (2012) 443–447.

[30] S. Zhang, Y.Q. Hou, H. Fujii, T. Onishi, M. Kokubu, M. Obata, H. Tanno, T. Kono, H. Uchiike, Effect of nonstoichiometry on the deterioration of Eu^{2+}-doped hexagonal aluminate phosphor for plasma display applications, Japanese Journal of Applied Physics 42 (2003) 477–480.

[31] J. Zhang, L. Zhang, Z. Tang, Z. Zhang, T. Wang, Luminescent properties of $(Ce_{0.67}Tb_{0.33})Mn_xMg_{1-x}Al_{11}O_{19}$ phosphor in VUV region, Ceramics International 29 (2003) 583–586.

[32] B. Howe, A.L. Diaz, Characterization of host-lattice emission and energy transfer in $BaMgAl_{10}O_{17}$:Eu^{2+}, Journal of Luminescence 109 (2004) 51–59.

[33] V. Singh, R.P.S. Chakradhar, J.L. Rao, H.Y. Kwak, Photoluminescence and studies of $BaMgAl_{10}O_{17}$:Eu^{2+} phosphor with blue-emission synthesized by the solution combustion method, Journal of Luminescence 131 (2011) 1714–1718.

[34] T. Matsuzawa, Y. Aoki, N. Takeuchi, Y. Murayama, A new long phosphorescent phosphor with high brightness $SrAl_2O_4$:Eu^{2+},Dy^{3+}, Journal of the Electrochemical Society 143 (1998) 2670–2673.

[35] D. Wang, Q.R. Yin, Y.X. Li, M.Q. Wang, Concentration quenching of Eu^{2+} in $SrO{\cdot}Al_2O_3$:Eu^{2+} phosphor, Journal of Luminescence 97 (2002) 1–6.

[36] A. Douy, M. Capron, Crystallization of spray-dried amorphous precursors in the $SrO–Al_2O_3$ system: a DSC study, Journal of the European Ceramic Society 23 (2003) 2075–2081.

[37] T. Aitasalo, J. Holsa, M. Lastusaari, J. Legendziewicz, J. Niittykoski, Persistent luminescence of Eu^{2+} and Na^+ doped alkaline earth aluminates, Radiation Effects and Defects in Solids 158 (2003) 89–96.

[38] T.Y. Peng, H.P. Yang, X.L. Pu, B. Hu, Z.C. Jiang, C.H. Yan, Combustion synthesis and photoluminescence of $SrAl_2O_4$:Eu,Dy phosphor nanoparticles, Materials Letters 58 (2004) 352–356.

[39] H. Zhong, X. Zeng, Preparation of MAl_2O_4:Eu^{2+},Sm^{3+} (M = Ca, Sr, Ba) phosphors by the combustion method and their luminescent properties, South African Journal of Chemistry 61 (2008) 22–25.

[40] M. Ayvacikli, A. Ege, S. Yerci, N. Can, Synthesis and optical properties of Er^{3+} and Eu^{3+} doped $SrAl_2O_4$ phosphor ceramic, Journal of Luminescence 131 (2011) 2432–2439.

[41] R.F. Zheng, L. Xu, W.F. Qin, J.S. Chen, B.A. Dong, L.G. Zhang, H.W. Song, Electrospinning preparation and photoluminescence properties of $SrAl_2O_4$:Ce^{3+} nanowires, Journal of Materials Science 46 (2011) 7517–7524.

[42] Y. Liu, C.-N. Xu, Influence of calcining temperature on photoluminescence and triboluminescence of europium-doped strontium aluminate particles prepared by sol–gel process, Journal of Physical Chemistry B 107 (2003) 3991–3995.

[43] P. Zhang, M. Xu, Z. Zheng, L. Liu, L. Li, Synthesis and characterization of europium-doped $Sr_3Al_2O_6$ phosphors prepared by sol–gel technique, Journal of Sol–Gel Science and Technology 43 (2007) 59–64.

[44] P. Zhang, M.X. Xu, L. Liu, L.X. Li, Luminescent properties of $Sr_3Al_2O_6$:Eu,Pr prepared by sol–gel method, Journal of Sol–Gel Science and Technology 50 (2009) 267–270.

[45] S.K. Sharma, S.S. Pitale, M.M. Malik, M.S. Qureshi, R.N. Dubey, Spectral and kinetic characterization of orange-red emitting $Sr_3Al_2O_6$:Eu^{3+}/Sm^{3+} phosphor, Journal of Alloys and Compounds 482 (2009) 468–475.

[46] C.K. Chang, W. Li, X.J. Huang, Z.Y. Wang, X. Chen, X. Qian, R. Guo, Y.L. Ding, D.L. Mao, Photoluminescence and afterglow behaviour of Eu^{2+}, Dy^{3+} and Eu^{3+}, Dy^{3+} in $Sr_3Al_2O_6$ matrix, Journal of Luminescence 130 (2010) 347–350.

[47] S. Chawla, A. Yadav, Role of valence state of dopant (Eu^{2+}, Eu^{3+}) and growth environment in luminescence and morphology of $SrAl_{12}O_{19}$ nano- and microcrystals, Materials Chemistry and Physics 122 (2010) 582–587.

[48] M. Karmaoui, M.G. Willinger, L. Mafra, T. Herntrich, N. Pinna, A general nonaqueous route to crystalline alkaline earth aluminate nanostructures, Nanoscale 1 (2009) 360–365.

[49] N.K. Giri, S.K. Singh, D.K. Rai, S.B. Rai, $SrAl_4O_7$:Tm^{3+}/Yb^{3+} nanocrystalline blue phosphor: structural, thermal and optical properties, Applied Physics B 99 (2010) 271–277.

[50] H.N. Luitel, T. Watari, T. Torikai, M. Yada, Luminescent properties of Cr^{3+} doped $Sr_4Al_{14}O_{25}$:Eu/Dy blue-green and red phosphor, Optical Materials 31 (2009) 1200–1204.

[51] L.Y. Deng, Y.H. Hu, Y.H. Wang, H.Y. Wu, W. Xie, Influence of doping of Dy^{3+}/Nd^{3+} on the trap levels of $Sr_4Al_{14}O_{25}$:Eu^{2+}, Acta Physica Sinica 59 (2010) 3402–3407.

[52] S. Sakirzanovas, A. Katelnikovas, D. Dutczak, A. Kareiva, T. Justel, Synthesis and Sm^{2+}/Sm^{3+} doping effects on photoluminescence properties of $Sr_4Al_{14}O_{25}$, Journal of Luminescence 131 (2011) 2255–2262.

[53] W. Xie, Y.H. Wang, Y.H. Hu, H.Y. Wu, L.Y. Deng, Structure and luminescence properties of $Sr_4Al_{14}O_{25}$:Eu^{2+}/Dy^{3+} by Ba^{2+} substitution, Rare Metal Materials and Engineering 40 (2011) 921–926.

[54] C.J. Brinker, G.W. Scherer, Sol–Gel Science: The Physics and Chemistry of Sol–Gel Processing, Academic Press, London, 1990.

[55] B.L. Cushing, V.L. Kolesnichenko, C.J. O'Connor, Recent advances in the liquid-phase syntheses of inorganic nanoparticles, Chemical Reviews 104 (2004) 3893–3946.

[56] A. Katelnikovas, J. Barkauskas, F. Ivanauskas, A. Beganskiene, A. Kareiva, Aqueous sol–gel synthesis route for the preparation of YAG: evaluation of sol–gel process by mathematical regression model, Journal of Sol–Gel Science and Technology 41 (2007) 193–201.

[57] J.D. Mackenzie, E.P. Bescher, Chemical routes in the synthesis of nanomaterials using the sol–gel process, Accounts of Chemical Research 40 (2007) 810–818.

[58] A. Kareiva, Aqueous sol–gel synthesis methods for the preparation of garnet crystal structure compounds, Materials Science (Medžiagotyra) 17 (2011) 428–437.
[59] K. Vishista, F.D. Gnanam, Microstructural development of $SrAl_{12}O_{19}$ in alumina-strontia composites, Journal of the European Ceramic Society 29 (2009) 77–83.
[60] Y. Liu, Z.-F. Zhang, B. King, J. Halloran, R.M. Laine, Synthesis of yttrium aluminium garnet from yttrium and aluminium isobutyrate precursors, Journal of the American Ceramic Society 79 (1996) 385–394.
[61] N. Dubnikova, E. Garskaite, A. Beganskiene, A. Kareiva, Sol–gel synthesis and characterization of sub-microsized lanthanide (Ho, Tm, Yb, Lu) aluminium garnets, Optical Materials 33 (2011) 1179–1184.
[62] B. Schrader (Ed.), Infrared and Raman Spectroscopy: Methods and Applications, VCH, Weinheim, 1995.
[63] K. Nakamoto, Infrared and Raman Spectra of Inorganic and Coordination Compounds, John Wiley and Sons, New York, 1986.
[64] M. Chroma, J. Pinkas, I. Pakutinskiene, A. Beganskiene, A. Kareiva, Processing and characterization of sol–gel fabricated mixed metal aluminates, Ceramics International 31 (2005) 1123–1130.
[65] S. Cizauskaite, S. Johnsen, J.-E. Jørgensen, A. Kareiva, Sol–gel preparation and characterization of non-substituted and Sr-substituted gadolinium cobaltates, Materials Chemistry and Physics 125 (2011) 469–473.
[66] A. Katelnikovas, H. Bettentrup, D. Uhlich, S. Sakirzanovas, T. Justel, A. Kareiva, Synthesis and optical properties of Ce^{3+}-doped $Y_3Mg_2AlSi_2O_{12}$ phosphors, Journal of Luminescence 129 (2009) 1356–1361.
[67] A. Katelnikovas, J. Jurkevicius, K. Kazlauskas, P. Vitta, T. Jüstel, A. Kareiva, A. Zukauskas, G. Tamulaitis, Efficient cerium-based sol–gel derived phosphors in different garnet matrices for light-emitting diodes, Journal of Alloys and Compounds 509 (2011) 6247–6251.
[68] G. Blasse, B.C. Grabmaier, Luminescent Materials, Springer-Verlag, Berlin, 1994.
[69] Z.-X. Fang, L.-X. Ning, Z.-F. Cui, First principles study on the 4f–5d transition of Ce^{3+} in $LuAlO_3$, Chinese Journal of Chemical Physics 24 (2011) 134–140.